High-speed and long-time growth of GaN by suppressing gas-phase reaction in the oxide vapor phase epitaxy method

Shigeyoshi Usami[1]*, Ayumu Shimizu[1], Ritsuko Higashiyama[1], Masayuki Imanishi[1], Junichi Takino[2], Tomoaki Sumi[2], Yoshio Okayama[2], Maruyama Mihoko[1], Masashi Yoshimura[3] Masahiko Hata[4], Masashi Isemura[5] and Yusuke Mori[1]

[1]*Graduate School of Engineering, Osaka University, Suita, Osaka 565-0871, Japan*

[2]*Panasonic Holdings Corporation, Kadoma, Osaka 571-8502, Japan*

[3]*Institute of Laser Engineering, Osaka University, Suita, Osaka 565-0871, Japan*

[4]*Itochu Plastics Inc., Chiyoda-ku, Tokyo 102-0082, Japan*

[5]*Sosho-Ohshin Inc., Suita, Osaka 565-0871, Japan*

E-mail: usami@eei.eng.osaka-u.ac.jp

In the growth of GaN using the oxide vapor phase epitaxy (OVPE) method, the issue of polycrystallization was likely to occur during high-speed growth owing to the high reactivity of Ga_2O and NH_3. Previous studies have shown that polycrystallization can be reduced by suppressing the gas-phase reactions. Recent thermodynamic analysis has predicted that gas-phase reactions can be further suppressed while maintaining high growth rates in the low V/III ratio region with a high Ga_2O flow rate and a low NH_3 flow rate. In this study, we performed crystal growth in the predicted region and verified the suppression of gas-phase reactions. Under conventional conditions, polycrystallization occurred when grown for a long time at a growth rate of 200 μm/h, but by applying growth conditions close to the predicted region, polycrystallization during long-time growth was suppressed, and a 1 mm thick GaN crystal was obtained.

1. Introduction

GaN has attracted attention as a material for high-efficiency power devices owing to its high breakdown electric field, electron mobility, and saturation electron velocity[1)-3)]. However, its high production cost has hindered the widespread use of GaN-based power devices; one reason for the high production cost of GaN is the lack of a high-speed fabrication method for ingots, such as the Czochralski process used for Si. Currently, hydride vapor phase epitaxy (HVPE), which has the highest growth rate, is the most commonly used method for fabricating freestanding GaN wafers[4)-11)]. However, the HVPE method poses a challenge for long-term growth because of the solid byproduct, NH_4Cl[12)]. NH_4Cl is produced in the exhaust section by the reaction of the source gases, HCl and NH_3 and causes blockages in the exhaust pipe of the reactor. To overcome this problem, we proposed an oxide vapor phase epitaxy (OVPE) method that uses gallium suboxide (Ga_2O) gas as a group-III source[13)-15)]. The reaction for the formation of Ga_2O and GaN using the OVPE method are as follows[13)-19)]:

$$2Ga(l) + H_2O(g) \rightarrow Ga_2O(g) + H_2(g) \quad (1)$$

$$Ga_2O(g) + 2NH_3(g) \rightarrow 2GaN(s) + 2H_2(g) + H_2O(g) \quad (2)$$

The water (H_2O) vapor does not produce solid byproducts when mixed with NH_3. Therefore, the OVPE method achieves long-term growth. In addition, the OVPE method does not require neutralization facilities because it is an HCl-free process. Furthermore, free-standing GaN wafers produced by the OVPE method exhibit very low resistivity[20)]. This was due to the heavy doping of oxygen from Ga_2O into GaN. These features make the OVPE a particularly advantageous method for reducing the cost of GaN wafers for vertical power devices.

However, because of the high reactivity of Ga_2O and NH_3, the OVPE method suffers from polycrystallization when the growth rate is increased[15)]. In response to this issue, we reported that polycrystallization can be suppressed by reducing the gas-phase reaction. By adjusting the partial pressure of NH_3 and H_2 and increasing the growth temperature, the gas-phase reaction can be reduced, and we have achieved a growth rate of up to 195 μm/h while suppressing polycrystallization[20)-22)]. Recently, thermodynamic analyses have predicted high-speed growth conditions under which further suppression of gas-phase reactions is possible[23)]. The predictions derived from the thermodynamic analysis are as follows:

- Reducing the NH_3 concentration was expected to dramatically suppress the gas-phase reaction; however, the growth rate also decreased.

- Even with a low NH_3 supply, a high growth rate could be achieved while suppressing the gas-phase reaction by increasing the Ga_2O supply.

Therefore, compared to previous studies, it is necessary to reduce the NH_3 supply and increase the Ga_2O supply. In this study, we investigated whether it is possible to grow GaN at a high speed for a long time while suppressing polycrystallization under the growth conditions predicted by thermodynamic analysis.

2. Experimental methods

GaN was grown using the OVPE method in a horizontal quartz reactor. The schematic is shown in Fig. 1. For synthesizing Ga_2O gas, liquid Ga (6N) and N_2O gas (5N) were used. NH_3 (6N) was used as a source for group V. A mixture of nitrogen (5N) and hydrogen (6N) was used as carrier gas. N_2O was used to generate H_2O vapor in the reactor. As N_2O is unstable at high temperatures[24], it decomposes immediately into N_2 and O_2 upon entering the heated reactor, which then reacts with the H_2 carrier gas to be converted into H_2O vapor. The conversion efficiency from N_2O to Ga_2O was determined by calculating the Ga_2O flow rate based on the decrease in Ga weight before and after growth. In this calculation, it was assumed that all the lost Ga was converted into Ga_2O. A commercially available free-standing GaN substrate was used as the seed substrate [full width at half maximum (FWHM) values of the X-ray rocking curve (XRC) for the 0002 and $10\bar{1}2$ diffractions were 54–80 and 54–66 arcsec, respectively]. The growth and source zones were heated to 1260 and 1100°C, respectively. A local heating system was used for heating above 1200°C (this system is explained in Ref. 22). To investigate the dependence of growth rate and amount of polycrystal on Ga_2O and NH_3 partial pressures, the flow rate of N_2O varied from 21.5 to 29.0 sccm, and the flow rate of NH_3 varied from 50 to 150 sccm. As the partial pressure of H_2 affects the growth rate[23),25)], the H_2 flow rate of the carrier gas was adjusted such that the partial pressure of H_2 in the growth zone remained nearly constant at 0.4 atm. The total gas flow rate, excluding N_2O, was fixed at 4500 sccm, and the growth was performed under atmospheric pressure (1 atm). The growth time was 30 min. Under the previously reported (conventional) conditions, the Ga_2O, NH_3, and total flow rates were 11, 1000, and 5700 sccm, respectively[22]. The conditions for this study, as shown above, were selected such that the Ga_2O flow rate was higher and the NH_3 flow rate was lower than those under conventional conditions. The maximum flow rate of N_2O was set at 29.0 sccm to maintain its concentration below the explosion limit. The growth rate was measured from the cross-sectional scanning electron microscopy (SEM; Keyence, VHX-D510) images, and the

amount of polycrystals was quantified from the surface SEM images as the ratio of the area of polycrystals to the substrate area (defined as "polycrystal coverage"). The obtained polycrystal coverage and growth-rate dependence on the Ga_2O and NH_3 flow rates were used to derive conditions suitable for long-term growth, at which point the growth time was extended to 5 h. The polycrystal coverage and growth thickness after long-term growth were compared with those obtained under conventional conditions to verify the effect of reduced gas-phase reactions on long-term growth. The crystallinity, electrical property, and impurity concentration of the obtained GaN crystals were evaluated using X-ray diffraction (XRD; Rigaku, SmartLab-RS, Cu Kα, 40 kV, 30 mA), Hall measurement (Toyo Technica, Resitest 8400), and secondary ion mass spectroscopy (SIMS), respectively.

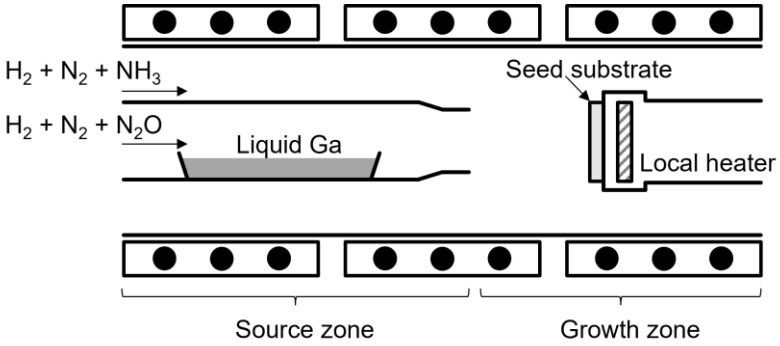

Fig. 1 Schematic of a horizontal OVPE growth reactor.

3. Results and discussion

3.1 Dependence of growth rate and polycrystal coverage on Ga_2O, NH_3 flow rates

Figure 2(a) shows the NH_3 flow rate dependence of the growth rate and polycrystal coverage on the NH_3 flow rate, where the N_2O flow rate was maintained at 24.5 sccm. Bird's-eye view SEM images of GaN crystals grown at NH_3 flow rates of 150 and 100 sccm are shown in Figs. 2(b) and 2(c), respectively. The conversion efficiency of N_2O to Ga_2O was 60%–61.6%, resulting in a Ga_2O flow rate of approximately 15 sccm. The growth rates decreased from 230 to 106 μm/h with decreasing NH_3 flow rates. Notably, almost no polycrystallization occurred at NH_3 flow rates of 100 sccm. This finding suggests that low NH_3 flow rate can effectively suppress gas-phase reactions while concomitantly reducing the driving force (supersaturation) for crystal growth.

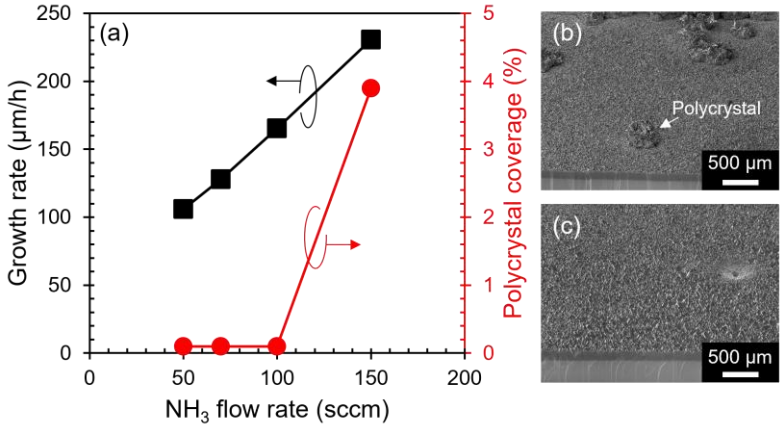

Fig. 2 (a) NH_3 flow rate dependence of the growth rate and polycrystal coverage on the NH_3 flow rate, with the N_2O flow rate maintained at 24.5 sccm. The bird's-eye view SEM images of the GaN crystals grown at NH_3 flow rates of (b) 150 and (c) 100 sccm.

Figure 3(a) shows the relationship between the growth rate and Ga_2O flow rate while maintaining a constant NH_3 flow rate of 50 or 100 sccm. To enhance the Ga_2O flow rate, the N_2O flow rate was varied from 21.5 to 29.0 sccm. The conversion efficiency was 59.1%–61.6%. At an NH_3 flow rate of 100 sccm, the growth rate exhibited a monotonic increase, reaching 221 μm/h at a Ga_2O flow rate of 16.9 sccm. However, when the NH_3 flow rate was reduced to 50 sccm, the growth rate did not increase monotonically, and GaN growth became unstable. This instability is likely because when NH_3 is extremely low, the growth rate is strongly influenced by slight changes in the growth environment (such as growth temperature, gas distribution, and wafer position). The polycrystal coverage of the same crystal is shown in Fig. 3(b). At an NH_3 flow rate of 50 sccm, no polycrystal growth was observed. At an NH_3 flow rate of 100 sccm, the polycrystal coverage increased slightly to 0.6% at a Ga_2O flow rate of 16.9 sccm. Although this crystal had nearly the same growth rate as the crystal grown at the NH_3 flow rate of 150 sccm shown in Fig. 2(a), the polycrystal coverage was approximately one order of magnitude lower. This finding suggests that the gas-phase reaction was not promoted, even with an increased Ga_2O flow rate.

These results demonstrate that a growth rate of approximately 200 μm/h, equivalent to conventional conditions[22], can be attained while suppressing polycrystallization in the region predicted by thermodynamic calculations (low NH_3 flow rate and high Ga_2O flow rate). The V/III ratio, calculated as $2 \times Ga_2O$ (sccm) / NH_3 (sccm) under these conditions, was less than 4, which was 10 times lower than that under conventional conditions[22),26]. Further investigations with higher Ga_2O flow rates are required to determine the growth rates that can be achieved under these low NH_3 conditions. In this section, we demonstrate that high-speed growth can be achieved while suppressing polycrystallization at NH_3 flow

rates of 100 sccm or less and Ga_2O flow rates of approximately 16 sccm. The optimal Ga_2O and NH_3 flow rates also depend on the H_2 partial pressure, growth temperature, and pressure.

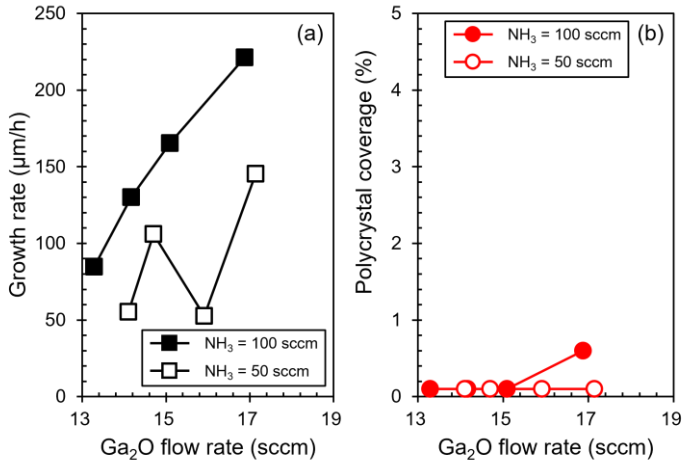

Fig. 3 (a) Growth rate vs. Ga_2O flow rate. (b) Polycrystalline coverage vs. Ga_2O flow rate. NH_3 flow rates were 50 or 100 sccm.

3.2 Long-time growth

Long-term growth was performed using two growth conditions under which no polycrystals were generated, as described in Section 3.1. The growth conditions are listed in Table 1. Condition A was defined as an NH_3 flow rate of 70 sccm, and condition B was defined as an NH_3 flow rate of 100 sccm. For comparison, long-term growth was performed under conventional conditions. Under conventional conditions with a high NH_3 flow rate, the reactor wall material was changed to tungsten for growth times of 2.5 h or more to avoid GaN deposition on the quartz tube. The conversion efficiency was approximately 60% under all conditions. Figures 4(a) and 4(b) show the growth-time dependence of the growth thickness and the polycrystal coverage of the obtained GaN crystals. Under both conventional conditions and condition B, a substantial amount of polycrystals was generated after 5 and 2.5 h of growth, respectively. As polycrystals were generated, the growth rate was observed to slow down. By contrast, almost no polycrystals were generated under condition A, the growth rate was maintained at approximately 200 μm/h, and the growth thickness reached 1 mm after 5 h of growth. This finding suggests that the NH_3 flow rates under conventional conditions and condition B were not sufficiently low to suppress the gas-phase reaction. It was also confirmed that condition A exhibited less parasitic deposition on the reactor walls than condition B (data not shown). This reduction in deposition was attributed to the suppression of the gas-phase reaction by

lowering the nucleation frequency[20),23)], which simultaneously inhibited heterogeneous nucleation on the reactor wall. Polycrystallization can also occur when microcrystals detached from parasitic deposits on the reactor wall attached to the growth surface. Therefore, the reduction in parasitic deposits may have also contributed to the suppression of polycrystallization under condition A. The relationship between parasitic deposition and polycrystallization warrants further investigation. Under Condition A, polycrystallization was suppressed to some extent during the long-term growth; however, numerous large pits were observed, and growth thickness decreased locally, as shown in Figs. 4(c) and 4(d). The exact cause of these large pits remains unknown, but is likely attributable to the adhesion of microcrystals nucleated in the gas phase or on the reactor walls, or potential contamination of the substrate.

Table 1. Growth conditions for long-time growth

	N_2O / Ga_2O flow rate (sccm)	NH_3 flow rate (sccm)	H_2 partial pressure (atm)	Total flow rate (sccm) w/o N_2O	V/III ratio	Reactor wall material
Condition A	24.5 / 14.8	70	0.40	4500	2.4	Quartz
Condition B	23 / 14.2	100	0.40	4500	3.5	Quartz
Conventional condition[22)]	18 / 11.3	1000	0.65	5700	45	Quartz (1h), Tungsten (2.5h, 5h)

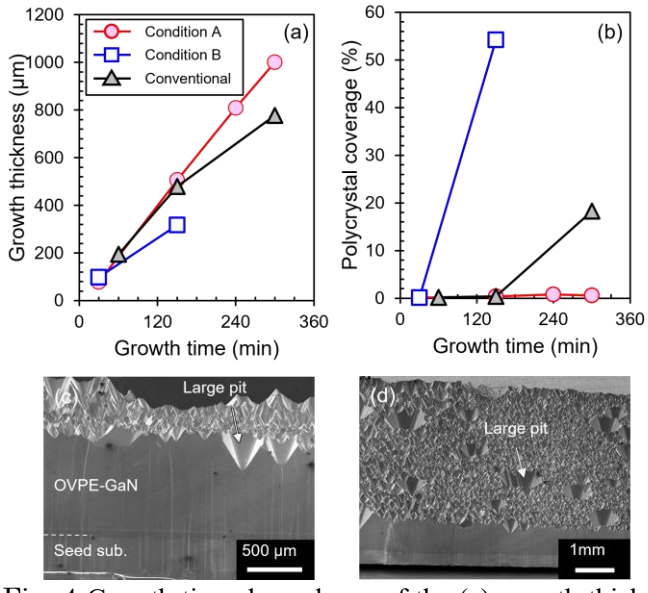

Fig. 4 Growth time dependence of the (a) growth thickness and (b) polycrystal coverage. (c) The cross-sectional and (d) bird's-eye view SEM image after 5 h of growth under condition A.

Under the conditions used in this study, the surfaces of all the crystals were covered with growth pits. Figure 5(a) shows the relationship between the growth pit density and film

thickness under all conditions, and Figs. 5(b)–5(d) show SEM images after 2.5 h of growth. Compared to conventional conditions, under Conditions A and B, the growth pits increased in size, and their density decreased as the growth thickness increased. In particular, under Condition A, which had the lowest V/III ratio, the density decreased to 3.8×10^4 cm^{-2} after 5 h of growth. Because threading dislocations bend along the facet plane[5),27)], they are concentrated at the center of the growth pits, leading to mutual annihilation and a low dislocation density[6),20),28)]. Condition A, which is characterized by the largest growth pit size, is suitable for producing wafers with a low dislocation density. A comparison between the inset in Fig. 5(b) and Fig. 5(d) reveals that the number of facets constituting the growth pits under Condition A is greater than that under the conventional condition. In the conventional condition, only the facet with an a-plane component (facet α) is observed, whereas under Condition A, in addition to facet α, a facet with an m-plane component (facet β) is also formed. It has been reported that facets α and β correspond to the $\{11\bar{2}2\}$ and $\{30\bar{3}4\}$ planes, respectively. This change in the facets of the growth pits is presumed to be related to the enlargement of the growth pits.

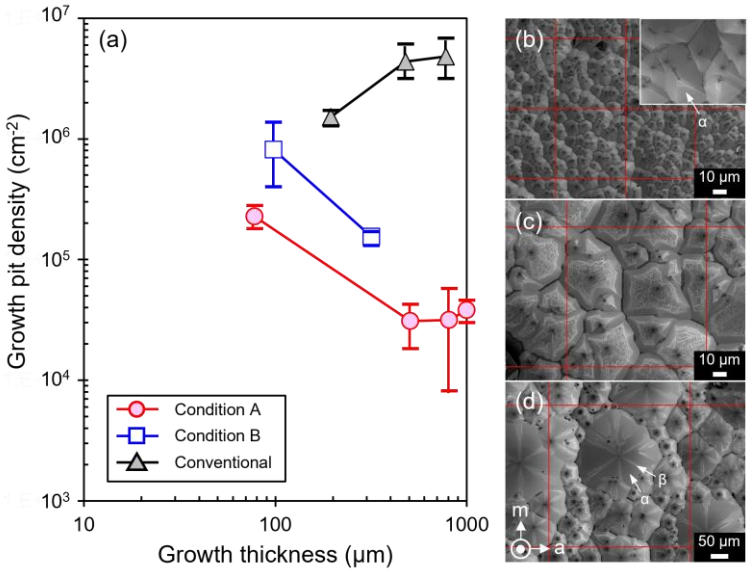

Fig. 5 (a) Relationship between growth pit density and film thickness. Surface SEM images of grown GaN crystals under (b) conventional condition, (c) Condition B, and (d) Condition A.

3.3 Evaluation of the obtained GaN crystal

In this section, we describe the properties of crystals grown under Condition A. The GaN crystals grown for 5 h were freestanded by chemical-mechanical polishing, and the XRC-FWHM and radius of curvature were evaluated using XRD. Consequently, the

FWHM of the 002 diffraction was 45 arcsec, and the radius of curvature was 30 m convex. This value is almost the same as that of the seed substrate. The crystals grown for 2.5 h were also processed into freestanding substrates and Hall and SIMS measurements were performed. The mobility, resistivity, and carrier concentration were 105 cm^2/Vs, 5.4×10^{-4} Ωcm, and 1.1×10^{20} cm^{-3}, respectively. This resistivity is the lowest ever achieved for OVPE-GaN[20),22),26),29)]. A comparison of impurity concentrations under conventional conditions is summarized in Table 2. The oxygen concentration was approximately three-fold higher than that under conventional conditions[22)]. Under Condition A, oxidant (N_2O) flow rate was 1.4 times higher than that in the conventional condition, and the NH_3 flow rate was reduced; therefore, the ratio of Group VI to Group V (VI/V ratio) increased, creating an environment in which oxygen could be doped more easily. The low hydrogen partial pressure was also related to an increase in the oxygen concentration[25)]. The hydrogen concentration increased by approximately 400 times compared with that under conventional conditions. Theoretically, it has been suggested that high-concentration oxygen doping increases the number of point defects[30),31)], and the existence of complex point defects consisting of oxygen at nitrogen sites and Ga vacancies (O_N-V_{Ga}) has also been experimentally demonstrated[32),33)]. Under condition A, the number of point defects increased with increasing oxygen concentration, and it was assumed that a large amount of hydrogen was incorporated into GaN, likely by terminating the dangling bonds of these point defects[34)]. When the ratio of carrier concentration to oxygen concentration is defined as the dopant activation rate, the values for the conventional condition and Condition A were 38% and 18%, respectively (see Table 2). The lower activation rate observed under Condition A, which contained a higher oxygen concentration, suggests that the number of point defects (interstitial oxygen or Ga vacancies) that act as compensating acceptors increased with increasing oxygen concentration[31)]. Under Condition A, the lowest resistivity was obtained in the OVPE owing to the high oxygen doping concentration while maintaining crystallinity. This low resistivity results in reduced conduction losses in vertical power devices. However, simultaneously, an increase in point defects was observed. Because an increase in point defects reduces thermal conductivity[35)], there is a concern regarding an increase in thermal resistance. Investigations of the thermal properties of OVPE-GaN are also necessary.

Table 2. Impurity concentration, carrier concentration and oxygen activation ratio in the grown crystals. The lower detection limit is indicated as DL.

	Oxygen (cm^{-3}) DL: 1×10^{16}	Hydrogen (cm^{-3})	Silicon (cm^{-3})	Carrier concentration	Dopant activation

		DL: 3×10^{16}	DL: 7×10^{14}	(cm^{-3})	ratio
Condition A	6.2×10^{20}	2.0×10^{19}	1.9×10^{17}	1.1×10^{20}	18%
Conventional condition[22)]	1.8×10^{20}	5.3×10^{16}	4.9×10^{18}	6.9×10^{19}	38%

4. Conclusions

In this study, we investigated the effect of reducing gas-phase reactions by growing GaN using the OVPE method under conditions that maintained a high growth rate and further suppressed gas-phase reactions, as predicted by thermodynamic analysis. We systematically varied the Ga_2O and NH_3 flow rates around the growth region predicted by thermodynamics to grow GaN, and obtained the following findings.

・Reducing the NH_3 flow rate reduced polycrystallization, but simultaneously reduced the growth rate.

・When the Ga_2O flow rate was increased at a low NH_3 flow rate, no significant polycrystallization was observed even at high growth rates exceeding 200 μm/h.

These trends are consistent with the predictions of the thermodynamic analysis and show that high-speed growth with suppressed gas-phase reactions is possible under low V/III ratios with reduced NH_3 flow rates and increased Ga_2O flow rates. When long-term growth was performed using these low V/III ratio conditions, polycrystallization was suppressed even after 5 h of growth, whereas in conventional methods, polycrystallization progressed as the growth time was extended, and a 1 mm thick GaN crystal was obtained. In addition, the grown GaN crystal was doped with a very high concentration of oxygen, 6.2×10^{20} cm^{-3}, which is three times higher than that of conventional methods, but the crystallinity was almost the same as that of the seed substrate. The high oxygen concentration resulted in a resistivity of 5.4×10^{-4} Ωcm, the lowest resistivity of any OVPE-GaN reported to date. This will lead to a reduction in the conduction loss in vertical power devices; however, the effect on thermal conductivity will need to be investigated in the future, owing to the decrease in the dopant activation rate. Through this research, it was shown that thick GaN crystals could be grown at high speeds using the OVPE method by applying low V/III ratio conditions that suppress gas-phase reactions.

Acknowledgments

This research was partly supported by the Ministry of the Environment, Japan, under the Project for Acceleration of Social Implementation and Dissemination of Components (GaN) and Materials (CNF) for Realizing Innovative CO_2 Emission Reduction and by JSPS KAKENHI (Grant No. JP23H00275).

References

1) T. Kachi, Jpn. J. Appl. Phys. **53**, 100210 (2014).
2) T. Ueda, M. Ishida, T. Tanaka, and D. Ueda, Jpn. J. Appl. Phys. **53**, 100214 (2014).
3) I.C. Kizilyalli, A.P. Edwards, O. Aktas, T. Prunty, and D. Bour, IEEE Trans. Electron Devices **62**, 414 (2015).
4) H.P. Maruska, and J.J. Tietjen, Appl. Phys. Lett. **15**, 327 (1969).
5) A. Usui, H. Sunakawa, A. Sakai, and A.A. Yamaguchi, Jpn. J. Appl. Phys. **36**, L899 (1997).
6) K. Motoki, T. Okahisa, N. Matsumoto, M. Matsushima, H. Kimura, H. Kasai, K. Takemoto, K. Uematsu, T. Hirano, M. Nakayama, S. Nakahata, M. Ueno, D. Hara, Y. Kumagai, A. Koukitu, and H. Seki, Jpn. J. Appl. Phys. **40**, L140 (2001).
7) Y. Oshima, T. Eri, M. Shibata, H. Sunakawa, and A. Usui, Phys. Status Solidi A **194**, 554 (2002).
8) K. Fujito, S. Kubo, H. Nagaoka, T. Mochizuki, H. Namita, and S. Nagao, J. Cryst. Growth **311**, 3011 (2009).
9) T. Yoshida, Y. Oshima, K. Watanabe, T. Tsuchiya, and T. Mishima, Phys. Status Solidi C **8**, 2110 (2011).
10) T. Sochacki, Z. Bryan, M. Amilusik, R. Collazo, B. Lucznik, J.L. Weyher, G. Nowak, B. Sadovyi, G. Kamler, R. Kucharski, M. Zajac, R. Doradzinski, R. Dwilinski, I. Grzegory, M. Bockowski, and Z. Sitar, Appl. Phys. Express **6**, 075504 (2013).
11) H. Fujikura, T. Konno, T. Suzuki, T. Kitamura, T. Fujimoto, and T. Yoshida, Jpn. J. Appl. Phys. **57**, 065502 (2018).
12) V. Voronenkov, N. Bochkareva, A. Zubrilov, Y. Lelikov, R. Gorbunov, P. Latyshev, and Y. Shreter, Phys. Status Solidi A **217**, 1900629 (2020).
13) Y. Bu, M. Imade, H. Kishimoto, M. Yoshimura, T. Sasaki, Y. Kitaoka, M. Isemura, and Y. Mori, J. Cryst. Growth **327**, 89 (2011).
14) M. Imade, H. Kishimoto, F. Kawamura, M. Yoshimura, Y. Kitaoka, T. Sasaki, and Y. Mori, J. Cryst. Growth **312**, 676 (2010).
15) M. Imade, Y. Bu, T. Sumi, A. Kitamoto, M. Yoshimura, T. Sasaki, M. Imsemura, and Y. Mori, J. Cryst. Growth **350**, 56 (2012).
16) P. Konkapaka, B. Raghothamachar, M. Dudley, Y. Makarov, and M.G. Spencer, J. Cryst. Growth **289**, 140 (2006).
17) A. Miura, S. Shimada, and T. Sekiguchi, J. Cryst. Growth **299**, 22 (2007).
18) T. Sumi, Y. Taniyama, H. Takatsu, M. Juta, A. Kitamoto, M. Imade, M. Yoshimura, M. Isemura, and Y. Mori, Jpn. J. Appl. Phys. **54**, 051001 (2015).
19) Y. Yamaguchi, Y. Taniyama, H. Takatsu, A. Kitamoto, M. Imade, M. Yoshimura, M. Isemura, and Y. Mori, Jpn. J. Appl. Phys. **55**, 05FB04 (2016).
20) 1) J. Takino, T. Sumi, Y. Okayama, M. Nobuoka, A. Kitamoto, M. Imanishi, M. Yoshimura,

and Y. Mori, Jpn. J. Appl. Phys. **58**, SC1043 (2019).

21) A. Shimizu, S. Tsuno, M. Kamiyama, K. Ishibashi, A. Kitamoto, M. Imanishi, M. Yoshimura, M. Hata, M. Isemura, and Y. Mori, Appl. Phys. Express **13**, 095504 (2020).
22) A. Shimizu, S. Usami, M. Kamiyama, I. Kawanami, A. Kitamoto, M. Imanishi, M. Maruyama, M. Yoshimura, M. Hata, M. Isemura, and Y. Mori, Appl. Phys. Express **15**, 035503 (2022).
23) Y. Sakurai, S. Usami, M. Imanishi, T. Sumi, J. Takino, Y. Okayama, M. Maruyama, M. Yoshimura, M. Hata, M. Isemura, and Y. Mori, J. Appl. Phys. **134**, 085704 (2023).
24) G. Löffler, L. Löffler, V.J. Wargadalam, F. Winter, and H. Hofbauer, Combust. Flame **120**, 427 (2000).
25) Y. Bu, M. Imade, A. Kitamoto, M. Yoshimura, M. Isemura, and Y. Mori, J. Cryst. Growth **392**, 1 (2014).
26) J. Takino, T. Sumi, Y. Okayama, M. Nobuoka, A. Kitamoto, M. Imanishi, M. Yoshimura, and Y. Mori, Jpn. J. Appl. Phys. **58**, SC1043 (2019).
27) K. Hiramatsu, K. Nishiyama, M. Onishi, H. Mizutani, M. Narukawa, A. Motogaito, H. Miyake, Y. Iyechika, and T. Maeda, J. Cryst. Growth **221**, 316 (2000).
28) T. Yoshida, and M. Shibata, Jpn. J. Appl. Phys. **59**, 071007 (2020).
29) S. Usami, R. Higashiyama, M. Imanishi, J. Takino, T. Sumi, Y. Okayama, M. Yoshimura, M. Hata, M. Isemura, and Y. Mori, J. Appl. Phys. **136**, 085103 (2024).
30) T. Mattila, and R.M. Nieminen, Phys. Rev. B **54**, 16676 (1996).
31) A.F. Wright, J. Appl. Phys. **98**, 103531 (2005).
32) J. Oila, V. Ranki, J. Kivioja, K. Saarinen, P. Hautojärvi, J. Likonen, J.M. Baranowski, K. Pakula, T. Suski, M. Leszczynski, and I. Grzegory, Phys. Rev. B **63**, 045205 (2001).
33) A. Uedono, J. Takino, T. Sumi, Y. Okayama, M. Imanishi, S. Ishibashi, and Y. Mori, J. Cryst. Growth **570**, 126219 (2021).
34) J.L. Lyons, A. Alkauskas, A. Janotti, and C.G. Van de Walle, Phys. Status Solidi B **252**, 900 (2015).
35) T. Kawamura, R. Nishiyama, T. Akiyama, S. Usami, M. Imanishi, Y. Mori, and M. Yoshimura, J. Cryst. Growth **649**, 127948 (2025).